Title

Growth and electrical transport properties of La0.7Sr0.3MnO3 thin films on Sr2IrO4 single crystals



Journal

Physical Review B, 95(15)

ISSN

2469-9950

Authors

Moon, EJ

May, AF

Shafer, P

et al.

Publication Date

2017-04-01

DOI

10.1103/physrevb.95.155135

Peer reviewed

# Growth and electrical transport properties of $La_{0.7}Sr_{0.3}MnO_3$ thin films on $Sr_2IrO_4$ single crystals

E. J. Moon,[1] A. F. May,[2,*] P. Shafer,[3] E. Arenholz,[3] and S. J. May[1,†]

[1]*Department of Materials Science and Engineering, Drexel University, Philadelphia, Pennsylvania 19104, USA*

[2]*Materials Science and Technology Division, Oak Ridge National Laboratory, Oak Ridge, Tennessee 37381, USA*

[3]*Advanced Light Source, Lawrence Berkeley National Laboratory; Berkeley, California 94720, USA*

(Received 30 September 2016; revised manuscript received 26 February 2017; published 20 April 2017)

We report the physical properties of $La_{0.7}Sr_{0.3}MnO_3$ thin films on $Sr_2IrO_4$ single crystals. The manganite films are deposited using oxide molecular beam epitaxy on flux-grown (001)-oriented iridate crystals. Temperature-dependent magnetotransport and x-ray magnetic circular dichroism measurements reveal the presence of a ferromagnetic metallic ground state in the films, consistent with films grown on $SrTiO_3$ and $La_{0.3}Sr_{0.7}Al_{0.65}Ta_{0.35}O_3$. A parallel resistance model is used to separate conduction effects within the $Sr_2IrO_4$ substrate and the $La_{0.7}Sr_{0.3}MnO_3$ thin films, revealing that the measured resistance maximum does not correspond to the manganite Curie temperature but results from a convolution of properties of the near-insulating substrate and metallic film. The ability to grow and characterize epitaxial perovskites on $Sr_2IrO_4$ crystals enables a new route for studying magnetism at oxide interfaces in the presence of strong spin-orbit interactions.

DOI: 10.1103/PhysRevB.95.155135

## I. INTRODUCTION

The use of epitaxial interfaces to stabilize or manipulate physical properties of materials has played a central role in condensed-matter physics. In complex oxide heterostructures, considerable experimental and theoretical efforts over the past two decades have focused on exploiting interfaces to realize new electronic, magnetic, superconducting, and ferroelectric behaviors [1–8]. The most commonly studied interface is the film/substrate junction, which is an inevitable component of all epitaxial heterostructures. By growing films on a variety of substrates, the epitaxial strain state of the film can be tuned, inducing elastic deformations to the unit cell (uc) that result in nonbulklike rotations and/or distortions of the corner-connected $BO_6$ octahedra for $ABO_3$ perovskite films [9–11]. Additionally, mismatches in the octahedral behavior of the film and substrate can result in local changes to the $B$-O-$B$ bond angle and $B$-O bond length in the near-interfacial region of the film/substrate heterojunction [12–17]. These substrate-imposed modifications to the film's atomic structure can lead to significant modifications to functional properties [18,19] as well as lead to new ferroic or electronic states not observed in isocompositional bulk counterparts [20,21].

At present, the variety of commercially available substrates for epitaxial perovskite film growth is largely limited to a few material families—titanates, aluminates, gallates, and scandates—the majority of which are insulating, nonmagnetic, and consist of 3$d$ $B$-site cations or other cations with relatively low atomic numbers. This last feature serves as an obstacle for studying epitaxial junctions between 3$d$- and 5$d$-based perovskites, the latter of which are the subject of intense current interest owing to their large spin-orbit coupling [22–25]. The presence of significant spin-orbit coupling on one side of the interface can be expected to alter magnetic and electronic behaviors in the adjoined material. For example, chiral magnetic ordering and other novel spin textures have been observed in ultrathin 3$d$ transition-metal films on 5$d$ metallic substrates due to interfacial Dzyaloshinskii-Moriya interactions [26–28].

Understanding the effects of spin-orbit coupling on interfacial properties has motivated recent experimental studies of $Sr_{3n-1}Ir_nO_{3n+1}$-based heterostructures, which have been carried out utilizing iridate films or superlattices [29–36]. Much of this work has focused on strain effects investigated by depositing iridate films on a variety of substrates, revealing a metal-insulator transition brought about by compressive strain in $SrIrO_3$ [37,38] and strain-induced changes to the band gap, Néel temperature, and optical absorption of $Sr_2IrO_4$ (SIO) [39–41]. The presence of anisotropic magnetoresistance (MR) within the $Sr_2IrO_4$ layer has been demonstrated in $Sr_2IrO_4/La_{0.7}Sr_{0.3}MnO_3$ bilayers arising from exchange coupling at the interface between the antiferromagnetic iridate and the ferromagnetic manganite [42]. The focus of these previous studies has been on the physical properties of the iridate layer; in contrast, there is limited understanding of how $Sr_2IrO_4$ alters the behavior of an adjoined layer in a heterostructure.

Here, we demonstrate the growth of manganite films on flux-grown $Sr_2IrO_4$ single crystals. The pseudocubic in-plane lattice parameter of $Sr_2IrO_4$ has been reported ranging from 3.878 to 3.888 Å [43–46], values between that of commonly used substrates $SrTiO_3$ [(STO), $a = 3.905$ Å] and $(LaAlO_3)_{0.3}(Sr_2AlTaO_6)_{0.7}$ [(LSAT), $a = 3.87$ Å]. The pseudocubic lattice parameters of bulk $La_{0.7}Sr_{0.3}MnO_3$ (LSMO) is 3.881 Å [47]. Thus, $Sr_2IrO_4$ can provide a closely lattice matched substrate for LSMO. Additionally, unlike $ABO_3$ perovskites, $A_2BO_4$ crystals can be cleaved yielding smooth (001) faces. We first confirm that the magnetic and electronic properties of the crystals are consistent with previous reports of $Sr_2IrO_4$. We then report on the structural, electronic, and magnetoresistive properties of 100-unit-cell-thick LSMO films deposited on the crystals using molecular-beam epitaxy. We demonstrate that ferromagnetic and metallic films can be realized in the $Sr_2IrO_4$ crystals, paving the way for future investigations of how the large spin-orbital coupling at the interface alters magnetism and magnetotransport at iridate/manganite junctions.

*mayaf@ornl.gov

†smay@coe.drexel.edu

 

## II. EXPERIMENTAL METHODS

$Sr_2IrO_4$ crystals were grown using a $SrCl_2$ flux in Pt crucibles. The starting materials $SrCO_3$, $IrO_2$, and $SrCl_2$, respectively, were combined in a 2:1:7 ratio. The Pt crucible was covered with a Pt lid and heated to 1300 °C. Upon reaching this maximum temperature, the furnace was slowly cooled (5 to 6 °C/h) to 900 °C and then to room temperature at 200 °C/h. Crystals were removed from the excess flux by boiling and sonicating in deionized water. This procedure resulted in the growth of crystals reaching 5 mm in dimension with typical dimensions on the order of 1–3 mm. These growth conditions are similar to those recently reported by Sung *et al.* [48]. In Ref. [48], the importance of minimizing dwell times at the maximum temperature was highlighted, and variations in crystal behavior with growth conditions were discussed.

To verify orientation and phase purity of the $Sr_2IrO_4$ crystals, x-ray diffraction data were collected on as-grown facets and on powder obtained by grinding several crystals. These data collections were performed using a PANalytical X'Pert Pro Multipurpose Diffractometer with a Cu $K_{\alpha,1}$ ($\lambda = 1.5406$ Å) incident beam monochromator. Rietveld refinements were performed using FULLPROF [49]. Magnetization measurements on single crystals were performed in a Quantum Design Magnetic Property Measurement System with data collected while cooling in an applied field.

LSMO thin films were grown with oxide molecule-beam epitaxy in an interrupted epitaxial growth mode on STO and LSAT substrates (MTI Corporation) and single-crystal SIO. The substrates were mounted adjacent to one another enabling simultaneous deposition on the crystals. The substrate temperature was held at ≈620 °C, and the ozone/oxygen mixture (∼5/95%) was sourced to the substrate at a rate that yielded a chamber pressure of $\approx 8 \times 10^{-6}$ Torr. The atomic fluxes for the cation deposition and the film thickness were calibrated using Rutherford backscattering spectrometry and x-ray reflectivity (XRR), respectively.

X-ray diffraction (XRD) measurements were taken around the 002 (pseudocubic notation) truncation rod of the film with a Rigaku Smartlab diffractometer, equipped with a parabolic mirror and a two-bounce/axis monochromator on the incident and diffracted beams. X-ray reflectivity data were fit using the GenX program [50]. Magnetotransport properties were measured in a Quantum Design Physical Property Measurement System. Transport measurements were carried out in a four-point geometry for the films on STO and LSAT. Due to the presence of surface features, such as terraces, large steps, and cracks that break lateral film continuity, two-point probe measurements were carried out on the LSMO/SIO samples with a lateral distance of less than approximately 0.1 mm between the contacts. Magnetoresistance measurements were carried out with the magnetic field applied perpendicular to the plane of the film ($H||c$). Soft x-ray spectroscopy was performed in the Vector Magnet at beamline 4.0.2 of the Advanced Light Source. Sample geometry was 20° from grazing, and a magnetic field of 0.3 T was applied along the x-ray beam direction for x-ray magnetic circular dichroism (XMCD) measurements. Each XMCD curve is the average of 16 measurements in which the circular polarization of the incoming x rays was reversed for subsequent scans. Data were collected in total electron yield mode and normalized to the intensity of incident x rays. The absorption intensity was normalized further to the resonant edge jump (the difference between the $L_3$ peak intensity and the preedge background) in the usual manner to allow quantitative comparisons between samples.

## III. RESULTS

### A. Properties of bulk $Sr_2IrO_4$

The quality of a film or heterostructure is dependent on the quality of the substrate. This investigation has utilized laboratory-grown single crystals as substrates, and thus it is essential to establish the properties of these crystals and demonstrate the reproducibility of such results. As such, a variety of measurements was performed to demonstrate that the $Sr_2IrO_4$ crystals are indeed consistent and of high quality. To summarize, from a bulk perspective, the x-ray diffraction, transport, and magnetic measurements indicate that the $Sr_2IrO_4$ crystals utilized here as substrates appear to be of high quality and are generally consistent between and within different growths.

Powder x-ray diffraction data from a collection of ground single crystals are shown in Fig. 1. Rietveld refinement was performed to assess the phase purity and crystal structure, and all peaks are well accounted for using the tetragonal space-group $I4_1/acd$ (number 142) reported by Crawford *et al.* [43]. The refined lattice parameters of $a = 5.4928(2)$ and $c = 25.7990(10)$ Å agree well with those reported in Ref. [43], and the relevant parameter for epitaxial film growth is $a/\sqrt{2} = 3.8840$ Å. Whereas these results show sharp diffraction peaks and indicate high crystallinity, it is magnetization and transport measurements that provide a better probe of sample quality in $Sr_2IrO_4$.

The bulk magnetization ($M$) and resistance measurements shown in Fig. 2 were utilized to verify that the $Sr_2IrO_4$ substrates/crystals are of high quality. Growth conditions can

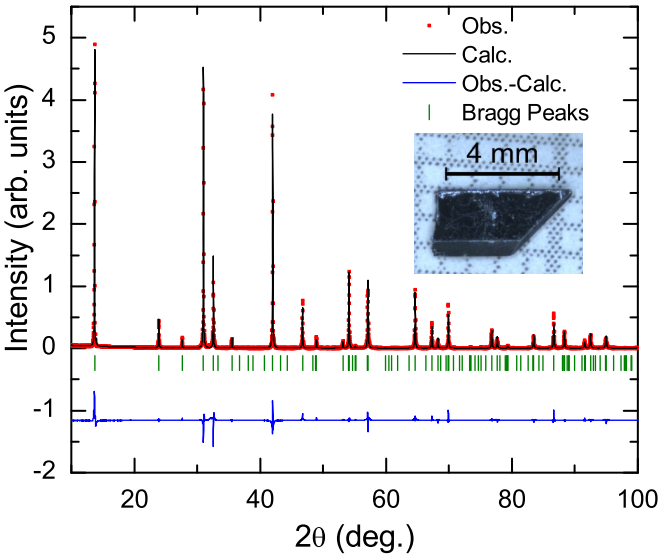


FIG. 1. Powder x-ray-diffraction data for ground crystals of $Sr_2IrO_4$. Rietveld refinement (labeled "Calc") demonstrates the desired phase purity and crystal structure.

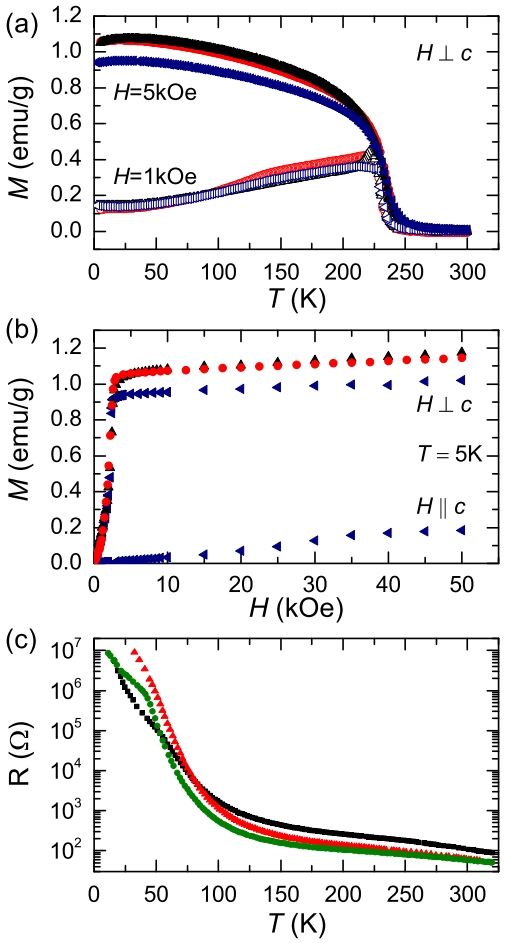


FIG. 2. (a) Temperature dependence of the magnetization for various $Sr_2IrO_4$ crystals; data collected upon cooling. These panels compare the behavior observed in various samples from multiple growth batches; the crystals are found to be consistent between and within different growths. (b) Isothermal magnetization curves for single-crystalline $Sr_2IrO_4$ demonstrating the critical field and anisotropy of the induced magnetization. (c) Electrical resistance within the $ab$ plane of various $Sr_2IrO_4$ crystals.

significantly influence the magnetic response of $Sr_2IrO_4$, particularly by changing the oxygen content as was demonstrated nicely in Ref. [48]. The temperature-dependent magnetization data shown in Fig. 2(a) are typical for $Sr_2IrO_4$, which possesses a canted antiferromagnetic ground state [51]. When measuring $M$ with a field applied within the $ab$ plane, $M(T)$ has a cusplike feature near 220 K if $H$ is below the critical field of approximately 3 kOe. When $H$ is greater than the critical field, a weak ferromagnetic state is observed due to alignment of the canted moments. As shown in Fig. 2(a), data collected with $H = 5$ kOe have a temperature dependence similar to that of a ferromagnet with a Curie temperature near 240 K. The magnetic anisotropy is shown in Fig. 2(b) where isothermal magnetization scans are presented. These results show the critical field near 3 kOe for $H \perp c$ and demonstrate that the magnetization is relatively hard for $H \parallel c$. At low $T$, the induced moment reaches $\approx 0.08 \mu_B$/Ir (note that 1 emu/g $= 0.0773 \mu_B$/Ir).

The electrical resistivity is another probe of sample quality in $Sr_2IrO_4$, and resistance data for representative $Sr_2IrO_4$ crystals are shown in Fig. 2(c). As with magnetization data, oxygen vacancies can significantly influence the temperature-dependent resistance data. In particular, oxygen vacancies promote metallic conduction in $Sr_2IrO_4$, and samples with the least oxygen deficiency generally appear to be the most insulating [45]. In comparison to the available literature, these $Sr_2IrO_4$ crystals appear to be of high quality with a large increase in resistance upon cooling. Demonstrating that the crystals become insulating at low $T$ is important for this study since the near-metallic state of $Sr_2IrO_4$ at high $T$ provides an additional conduction path when attempting to measure the electrical properties of epitaxial films grown on $Sr_2IrO_4$. The in-plane resistivity $\rho_{ab}$ of $Sr_2IrO_4$ is approximately 1 $\Omega$ cm at 300 K; the resistivity along the $c$ axis is about two orders of magnitude larger [45].

### B. Structural properties of manganite/iridate heterostructures

Figure 3(a) shows XRR data of LSMO films grown simultaneously on STO(001), LSAT(001), and SIO(001), respectively. The measured data were fit (solid lines) well to a model assuming a uniform scattering length density throughout the film. The fits confirm the thickness of the LSMO films to be approximately 100 uc. The reflectivity can be well fit using models with film/substrate roughness and surface roughness values of 0.2–0.7 nm for LSMO/STO and LSMO/LSAT; the roughness values of LSMO/SIO are larger on the order of 1.0–1.5 nm.

Figure 3(b) shows XRD measurements taken around the (002) (pseudocubic notation) diffraction peak of the LSMO

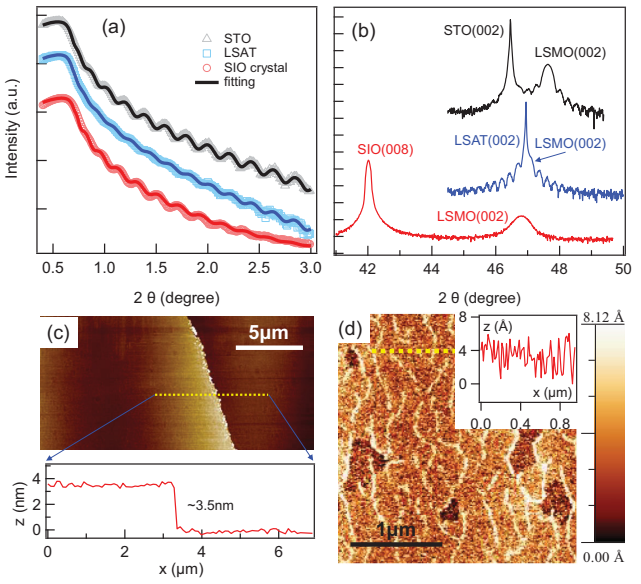


FIG. 3. (a) X-ray reflectivity measured from LSMO films grown on STO and LSAT substrates and a SIO crystal. The solid lines are the fits to a model by GENX software. (b) X-ray diffraction measured from LSMO films on STO and LSAT substrates and a SIO crystal. (c) Atomic force microscopy image showing a step height in the LSMO/SIO film and (d) an example region between the step heights; line scans obtained from the dotted yellow lines are shown in (c) and (d).

films. The LSMO/STO and LSMO/LSAT show the expected Bragg reflection for $c$-axis-oriented layers and clear Kiessig fringes testifying to the quality of the films. The lattice mismatches among LSMO and various substrate materials are 0.6% (STO), 0.1% (SIO), and −0.3% (LSAT) where a positive value indicates the film would be under tensile strain. The contraction of the $c$-axis parameters from 3.87 Å in LSMO/LSAT to 3.82 Å in LSMO/STO is consistent with changes in the lattice parameters that would be expected in strained films. In contrast, the film on a SIO crystal exhibits a broad peak, which is centered at $2\theta = 46.8^\circ$ ($c = 3.882$ Å). This $c$-axis parameter is not between that of LSMO/LSAT and LSMO/STO as would be anticipated for a strained film, suggesting that the LSMO/SIO film is at least partially relaxed.

The surface morphology of LSMO on SIO was investigated with atomic force microscopy. Images obtained from a specularly reflective region of a LSMO/SIO film are shown in Figs. 3(c) and 3(d). The surface morphology of the LSMO/SIO exhibits smooth regions separated by large step heights of 3 to 4 nm. An example step is shown in Fig. 3(c) along with a corresponding line scan. Figure 3(d) shows the morphology in a smooth region where surface roughness is one unit cell or less. We assign these large steps as the origin of the increased roughness measured in XRR and the broadening of the film diffraction peak. We suggest that these steps create planar defects through the film and may assist in strain relaxation that appears to have occurred within the film. We also note that there must exist larger steps, terraces, or cracks within the crystals that lead to lateral discontinuities within the film as transport measurements in which the contacts were placed at distances greater than ≈0.1 mm resulted in insulating behavior dominated by the substrate as opposed to the metallic conduction described below.

### C. Magnetotransport properties of manganite/iridate heterostructures

We next turn to dc transport measurements to elucidate the electronic properties of the films. Figure 4(a) shows the temperature dependence of the resistivity of the LSMO films grown on insulating LSAT and STO. These films are metallic, consistent with previous reported behavior of LSMO on these substrates, albeit with a local maximum at ∼310 K which is reduced from the near 350-K maximum observed in optimized LSMO [52–55]. In manganites, a resistivity maximum commonly is observed at or near the Curie temperature [56,57]. The temperature-dependent resistance of the LSMO/SIO sample is shown in Fig. 4(b). We do not attempt to convert the LSMO/SIO measured resistance into resistivity as the SIO substrate provides a parallel conduction path to the LSMO film. In contrast to the other two films grown simultaneously, the film on SIO exhibits a maximum at ∼250 K. To assist in the interpretation of the resistance data, we modeled the resistance ($R$) in the LSMO/SIO as resistors in parallel using $1/R = A_S/R_S + A_L/R_L$, where $R_S$ and $R_L$, respectively, are the measured resistances from the SIO crystal and LSMO film on STO and $A_S$ and $A_L$ are prefactors that would arise from geometric effects. Although we use the LSMO/STO resistance obtained from a four-point probe resistance measurement, we show results from a two-point probe measurement of the same

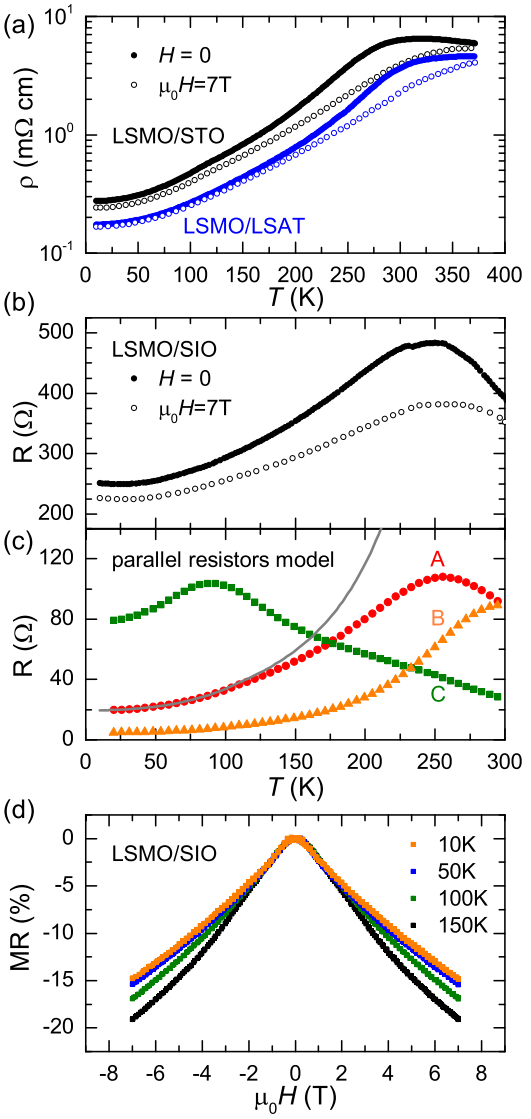


FIG. 4. Temperature-dependent resistivity measured in a zero magnetic field (filled symbols) and 7 T (open symbols) of LSMO films grown on (a) STO and LSAT substrates and (b) a SIO crystal. (c) Simulation results from the parallel resistor model obtained using $A_S = A_L = 1$ (curve A); $A_S = 1/4$, $A_L = 4$ (curve B); $A_S = 4$, $A_L = 1/4$ (curve C). The gray line in (c) is the absolute resistance measured for LSMO/STO presented in panel (a). (d) Field-dependent magnetoresistance measured from the LSMO/SIO sample.

sample in the Supplemental Material [58]. We obtained a nearly identical temperature dependence of the resistance for these two geometries confirming that the four-point resistance of LSMO on STO can be used in our parallel conduction model and that any temperature dependence to the contact resistance is a minimal effect.

This simple model reproduces the resistance maximum near 250 K when $A_S$ and $A_L$ are set to 1 as shown by curve A in Fig. 4(c), whereas modifying the prefactors $A_S$ and $A_L$ changes the location of the resistance maximum as shown by curves B and C. We note that the aim of this modeling is not to reproduce the exact magnitude of the resistance but instead to elucidate the nature of the local maximum in resistance. By reproducing this feature, we confirm that the resistance

maximum of LSMO/SIO arises from contributions in both LSMO and SIO and, therefore, the measured resistance maximum does not indicate the Curie temperature or the presence of a metal-insulator transition within the film. Instead, the model indicates that the resistance of the LSMO/SIO film follows a temperature dependence that is approximately the same as the LSMO/STO film, remaining metallic up to room temperature.

In Fig. 4(c), the gray line is the absolute resistance measured for LSMO/STO presented in Fig. 4(a). We used this resistance to represent the resistance of the LSMO film in the two-resistor model, although we note that the LSMO/STO measurement was carried out in a four-point geometry, and thus the effect of contact resistance is not included in the LSMO data used within the model. The data represented by black squares in Fig. 2(c) were used for the SIO resistance. At 100 K, this SIO crystal is approximately 50 times more resistive than the LSMO film on STO. Thus, although the exact proportions will vary with a particular crystal, electrical resistivity measurements can be considered to be dominated by the film below approximately 100 K. Indeed, the resistance of LSMO on STO and that of the simple model A converge below ≈125 K as shown in Fig. 4(c).

Field-dependent MR measurements from the LSMO/SIO sample, shown in Fig. 4(d), are also consistent with the transport occurring through the LSMO film below ≈150 K. The general field dependence of the MR curve and the reduction of MR with decreasing temperature is in agreement with previous reports of ferromagnetic manganites [59,60] and measurements of our LSMO/STO and LSMO/LSAT films. Whereas SIO also exhibits negative magnetoresistance, the field dependence of MR in SIO is markedly different from the LSMO/SIO film, namely, that bulk SIO exhibits the opposite concavity in MR as a function of field as what is shown in Fig. 4(d) [46,61]. In total, the measured resistance and magnetoresistance, interpreted through a parallel resistor model, indicate that the transport properties of LSMO on SIO are metallic up to temperatures of ∼310 K and that transport measurements below 125 K probe contributions from the LSMO layer with minimal conduction through the SIO crystal.

The magnetic properties of the films were investigated with XMCD in which the differences in the absorption of right and left circularly polarized x rays were measured at the Mn $L$-edge. Figure 5(a) shows the Mn $L$-edge XMCD spectrum of a LSMO film grown on SIO (red) and LSAT (black) measured at 300 K. The presence of a XMCD signal confirms ferromagnetic ordering persists to room temperature in both samples, although their relative strengths indicate a slightly lower Curie temperature for LSMO on SIO. The line shapes of the spectra are comparable to previously published data for this LSMO composition [62–64]. Furthermore, the $L_{2,3}$-edge peak position is the same for both samples, confirming that the nominal valence of the LSMO films is independent of the substrate for films of this thickness. The presence of ferromagnetism within the LSMO/SIO sample at 300 K supports our conclusion that 100-uc-thick LSMO films can be synthesized on SIO while still maintaining properties similar to LSMO/STO and LSMO/LSAT. Figure 5(b) displays the XMCD spectra at 80 K where the difference between LSMO/SIO and LSMO/LSAT is minimized compared to the 300-K data as both films are well below their Curie temperatures.

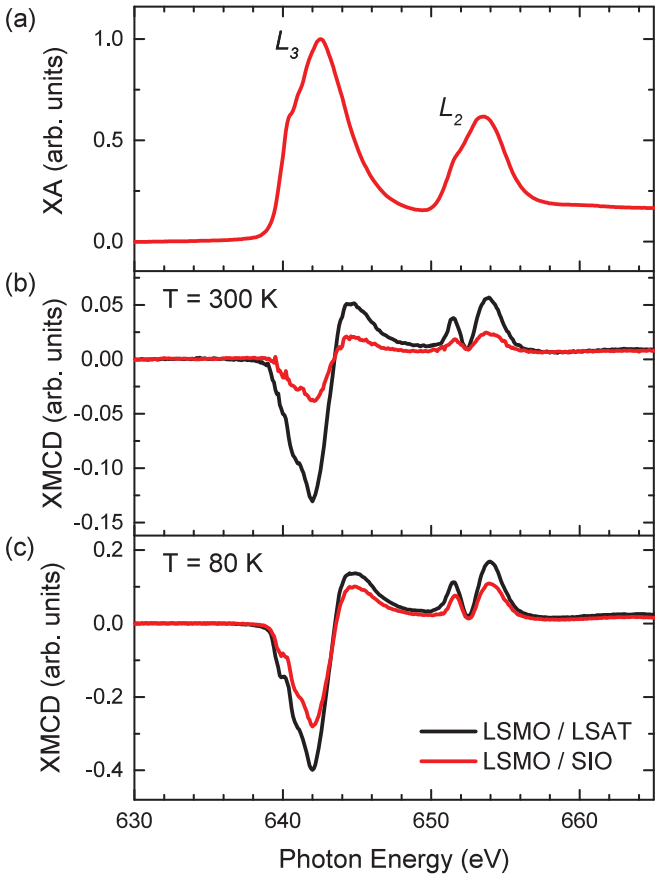


FIG. 5. Mn $L$-edge x-ray absorption (XA) and XMCD of LSMO grown on SIO (red) and LSAT (black). (a) XA at 80 K and XMCD at (b) 300 K and (c) 80 K.

## IV. DISCUSSION AND CONCLUSIONS

We have demonstrated that $Sr_2IrO_4$ single crystals can be used as substrates for the growth of $La_{0.7}Sr_{0.3}MnO_3$ films. The 100-uc-thick LSMO/SIO films exhibit comparable electronic and magnetic properties to films deposited simultaneously on commercial STO and LSAT substrates, which in turn exhibit properties that are consistent with bulk LSMO. In contrast to the STO and LSAT substrates, the SIO crystals are not completely insulating and act as a parallel channel for conduction in the LSMO/SIO heterostructures. We have shown that the experimentally obtained transport data from LSMO/SIO can be reproduced using a parallel resistor model, allowing us to conclude that the resistivity within the LSMO film remains metallic to temperatures well above the measured resistivity maximum from the LSMO/SIO heterostructure. These results are corroborated by XMCD measurements confirming the LSMO/SIO film is ferromagnetic at room temperature.

The ability to grow epitaxial perovskite films on single-crystal $Sr_2IrO_4$ enables a different approach for studying interfaces between 3$d$ and 5$d$ complex oxides, which to date have been fabricated using SIO layers grown by thin-film

deposition techniques. The use of SIO crystals as substrates allows for detailed characterization of the iridate prior to interface formation in order to confirm that the properties of the SIO are consistent with high quality stoichiometric bulk crystals. Starting with a well-characterized SIO crystal should enable better identification of intrinsic interfacial phenomena at SIO-based heterojunctions as opposed to defect-induced extrinsic behavior. We anticipate that epitaxial films on SIO crystals will provide a useful platform for exploring chiral magnetic states and novel spin textures in ultrathin magnetic oxide films, a topic that has attracted considerable interest in metallic magnetic interfaces but remains largely unexplored in oxide heterostructures [65].

## ACKNOWLEDGMENTS

A.F.M. was supported by the U.S. Department of Energy, Office of Science, Basic Energy Sciences, Materials Sciences and Engineering Division. E.J.M. and S.J.M. were supported by the U.S. Army Research Office under Grant No. W911NF-15-1-0133. The Advanced Light Source is supported by the Director, Office of Science, Office of Basic Energy Sciences, of the U.S. Department of Energy under Contract No. DE-AC02-05CH11231. We thank J. Yan for useful discussions. We are grateful to G. Karapetrov and M. Precner for access to the AFM instrument and assistance. A.F.M. and S.J.M. thank E. G. May for thought-provoking discussions.

[1] H. Y. Hwang, Y. Iwasa, M. Kawasaki, B. Keimer, N. Nagaosa, and Y. Tokura, Nature Mat. **11**, 103 (2012).
[2] K. S. Takahashi, M. Kawasaki, and Y. Tokura, Appl. Phys. Lett. **79**, 1324 (2001).
[3] A. Ohtomo, D. A. Muller, J. L. Grazul, and H. Y. Hwang, Nature (London) **419**, 378 (2002).
[4] A. Gozar, G. Logvenov, L. Fitting Kourkoutis, A. T. Bollinger, L. A. Giannuzzi, D. A. Muller, and I. Bozovic, Nature (London) **455**, 782 (2008).
[5] E. Bousquet, M. Dawber, N. Stucki, C. Lichtensteiger, P. Hermet, S. Gariglio, J. M. Triscone, and P. Ghosez, Nature (London) **452**, 732 (2008).
[6] B. Jalan, S. Stemmer, S. Mack, and S. J. Allen, Phys. Rev. B **82**, 081103(R) (2010).
[7] J. M. Rondinelli and C. J. Fennie, Adv. Mater. **24**, 1961 (2012).
[8] A. Bhattacharya and S. J. May, Annu. Rev. Mater. Res. **44**, 65 (2014).
[9] D. G. Schlom, L.-Q. Chen, C. J. Fennie, V. Gopalan, D. A. Muller, X. Pan, R. Ramesh, and R. Uecker, MRS Bull. **39**, 118 (2014).
[10] S. J. May, J.-W. Kim, J. M. Rondinelli, E. Karapetrova, N. A. Spaldin, A. Bhattacharya, and P. J. Ryan, Phys. Rev. B **82**, 014110 (2010).
[11] R. L. Johnson-Wilke, D. Marincel, S. Zhu, M. P. Warusawithana, A. Hatt, J. Sayre, K. T. Delaney, R. Engel-Herbert, C. M. Schleputz, J.-W. Kim, V. Gopalan, N. A. Spaldin, D. G. Schlom, P. J. Ryan, and S. Trolier-McKinstry, Phys. Rev. B **88**, 174101 (2013).
[12] C. L. Jia, S. B. Mi, M. Faley, U. Poppe, J. Schubert, and K. Urban, Phys. Rev. B **79**, 081405(R) (2009).
[13] A. Y. Borisevich, H. J. Chang, M. Huijben, M. P. Oxley, S. Okamoto, M. K. Niranjan, J. D. Burton, E. Y. Tsymbal, Y. H. Chu, P. Yu *et al.*, Phys. Rev. Lett. **105**, 087204 (2010).
[14] J. M. Rondinelli, S. J. May, and J. W. Freeland, MRS Bull. **37**, 261 (2012).
[15] R. Aso, D. Kan, Y. Shimakawa, and H. Kurata, Cryst. Growth Des. **14**, 2128 (2014).
[16] T. T. Fister, H. Zhou, Z. Luo, S. S. A. Seo, S. O. Hruszkewycz, D. L. Proffit, J. A. Eastman, P. H. Fuoss, P. M. Baldo, H. N. Lee, and D. D. Fong, APL Mater. **2**, 021102 (2014).
[17] A. Vailionis, H. Boschker, Z. Liao, J. R. A. Smit, G. Rijnders, M. Huijben, and G. Koster, Appl. Phys. Lett. **105**, 131906 (2014).
[18] E. J. Moon, P. V. Balachandran, B. J. Kirby, D. J. Keavney, R. J. Sichel-Tissot, C. M. Schleputz, E. Karapetrova, X. M. Cheng, J. M. Rondinelli, and S. J. May, Nano Lett. **14**, 2509 (2014).
[19] M. D. Biegalski, Y. Takamura, A. Mehta, Z. Gai, S. V. Kalinin, H. Ambaye, V. Lauter, D. Fong, S. T. Pantelides, Y. M. Kim, J. He, A. Borisevich, W. Siemons, and H. M. Christen, Adv. Mater. Interfaces **1**, 1400203 (2014).
[20] J. H. Haeni, P. Irvin, W. Chang, R. Uecker, P. Reiche, Y. L. Li, S. Choudhury, W. Tian, M. E. Hawley, B. Craigo, A. K. Tagantsev, X. Q. Pan, S. K. Streiffer, L. Q. Chen, S. W. Kirchoefer, J. Levy, and D. G. Schlom, Nature (London) **430**, 758 (2004).
[21] J. H. Lee, L. Fang, E. Vlahos, X. Ke, Y. W. Jung, L. Fitting Kourkoutis, J.-W. Kim, P. J. Ryan, T. Heeg, M. Roeckerath, V. Goian, M. Bernhagen, R. Uecker, P. C. Hammel, K. M. Rabe, S. Kamba, J. Schubert, J. W. Freeland, D. A. Muller, C. J. Fennie, P. Schiffer, V. Gopalan, E. Johnston-Halperin, and D. G. Schlom, Nature (London) **466**, 954 (2010).
[22] B. J. Kim, H. Jin, S. J. Moon, J.-Y. Kim, B.-G. Park, C. S. Leem, J. Yu, T. W. Noh, C. Kim, S.-J. Oh, J.-H. Park, V. Durairaj, G. Cao, and E. Rotenberg, Phys. Rev. Lett. **101**, 076402 (2008).
[23] G. Jackeli and G. Khaliullin, Phys. Rev. Lett. **102**, 017205 (2009).
[24] J. W. Kim, Y. Choi, J. Kim, J. F. Mitchell, G. Jackeli, M. Daghofer, J. van den Brink, G. Khaliullin, and B. J. Kim, Phys. Rev. Lett. **109**, 037204 (2012).
[25] S. Calder, J. W. Kim, G.-X. Cao, C. Cantoni, A. F. May, H. B. Cao, A. A. Aczel, M. Matsuda, Y. Choi, D. Haskel, B. C. Sales, D. Mandrus, M. D. Lumsden, and A. D. Christianson, Phys. Rev. B **92**, 165128 (2015).
[26] M. Bode, M. Heide, K. von Bergmann, P. Ferriani, S. Heinze, G. Bihlmayer, A. Kubetzka, O. Pietzsch, S. Blügel, and R. Wiesendanger, Nature (London) **447**, 190 (2007).
[27] S. Heinze, K. von Bergmann, M. Menzel, J. Brede, A. Kubetzka, R. Wiesendanger, G. Bihlmayer, and S. Blügel, Nat. Phys. **7**, 713 (2011).
[28] K.-W. Kim, H.-W. Lee, K.-J. Lee, and M. D. Stiles, Phys. Rev. Lett. **111**, 216601 (2013).
[29] J. S. Lee, Y. Krockenberger, K. S. Takahashi, M. Kawasaki, and Y. Tokura, Phys. Rev. B **85**, 035101 (2012).
[30] M. Uchida, Y. F. Nie, P. D. C. King, C. H. Kim, C. J. Fennie, D. G. Schlom, and K. M. Shen, Phys. Rev. B **90**, 075142 (2014).
[31] C. Lu, A. Quindeau, H. Deniz, D. Preziosi, D. Hesse, and M. Alexe, Appl. Phys. Lett. **105**, 082407 (2014).
[32] Y. F. Nie, P. D. C. King, C. H. Kim, M. Uchida, H. I. Wei, B. D. Faeth, J. P. Ruf, J. P. C. Ruff, L. Xie, X. Pan, C. J. Fennie, D. G. Schlom, and K. M. Shen, Phys. Rev. Lett. **114**, 016401 (2015).
[33] D. Hirai, J. Matsuno, and H. Takagi, APL Mater. **3**, 041508 (2015).

[34] J. Matsuno, K. Ihara, S. Yamamura, H. Wadati, K. Ishii, V. V. Shankar, H.-Y. Kee, and H. Takagi, Phys. Rev. Lett. **114**, 247209 (2015).
[35] J. Liu, D. Kriegner, L. Horak, D. Puggioni, C. Rayan Serrao, R. Chen, D. Yi, C. Frontera, V. Holy, A. Vishwanath, J. M. Rondinelli, X. Marti, and R. Ramesh, Phys. Rev. B **93**, 085118 (2016).
[36] T. J. Anderson, S. Ryu, H. Zhou, L. Xie, J. P. Podkaminer, Y. Ma, J. Irwin, X. Q. Pan, M. S. Rzchowski, and C. B. Eom, Appl. Phys. Lett. **108**, 151604 (2016).
[37] A. Biswas, K.-S. Kim, and Y. H. Jeong, J. Appl. Phys. **116**, 213704 (2014).
[38] L. Zhang, Q. Liang, Y. Xiong, B. Zhang, L. Gao, H. Li, Y. B. Chen, J. Zhou, S.-T. Zhang, Z.-B. Gu, S.-H. Yao, Z. Wang, Y. Lin, and Y.-F. Chen, Phys. Rev. B **91**, 035110 (2015).
[39] C. Rayan Serrao, J. Liu, J. T. Heron, G. Singh-Bhalla, A. Yadav, S. J. Suresha, R. J. Paull, D. Yi, J.-H. Chu, M. Trassin, A. Vishwanath, E. Arenholz, C. Frontera, J. Železný, T. Jungwirth, X. Marti, and R. Ramesh, Phys. Rev. B **87**, 085121 (2013).
[40] J. Nichols, J. Terzic, E. G. Bittle, O. B. Korneta, L. E. De Long, J. W. Brill, G. Cao, and S. S. A. Seo, Appl. Phys. Lett. **102**, 141908 (2013).
[41] A. Lupascu, J. P. Clancy, H. Gretarsson, Z. Nie, J. Nichols, J. Terzic, G. Cao, S. S. A. Seo, Z. Islam, M. H. Upton, J. Kim, D. Casa, T. Gog, A. H. Said, V. M. Katukuri, H. Stoll, L. Hozoi, J. van den Brink, and Y.-J. Kim, Phys. Rev. Lett. **112**, 147201 (2014).
[42] I. Fina, X. Marti, D. Yi, J. Liu, J. H. Chu, C. Rayan-Serrao, S. Suresha, and A. B. Shick, J. Železný, T. Jungwirth, J. Fontcuberta, and R. Ramesh, Nat. Commun. **5**, 4671 (2014).
[43] M. K. Crawford, M. A. Subramanian, R. L. Harlow, J. A. Fernandez-Baca, Z. R. Wang, and D. C. Johnston, Phys. Rev. B **49**, 9198 (1994).
[44] T. Shimura, Y. Inaguma, T. Nakamura, M. Itoh, and Y. Morii, Phys. Rev. B **52**, 9143 (1995).
[45] O. B. Korneta, T. Qi, S. Chikara, S. Parkin, L. E. De Long, P. Schlottmann, and G. Cao, Phys. Rev. B **82**, 115117 (2010).
[46] X. Chen, T. Hogan, D. Walkup, W. Zhou, M. Pokharel, M. Yao, W. Tian, T. Z. Ward, Y. Zhao, D. Parshall, C. Opeil, J. W. Lynn, V. Madhavan, and S. D. Wilson, Phys. Rev. B **92**, 075125 (2015).
[47] P. G. Radaelli, G. Iannone, M. Marezio, H. Y. Hwang, S.-W. Cheong, J. D. Jorgensen, and D. N. Argyriou, Phys. Rev. B **56**, 8265 (1997).
[48] N. H. Sung, H. Gretarsson, D. Proepper, J. Porras, M. Le Tacon, A. V. Boris, B. Keimer, and B. J. Kim, Philos. Mag. **96**, 413 (2016).
[49] J. Rodríguez-Carvajal, Physica B **192**, 55 (1993).
[50] M. Björck and G. Andersson, J. Appl. Crystallogr. **40**, 1174 (2007).
[51] B. J. Kim, H. Ohsumi, T. Komesu, S. Sakai, T. Morita, H. Takagi, and T. Arima, Science **323**, 1329 (2009).
[52] Y. Takamura, R. V. Chopdekar, E. Arenholz, and Y. Suzuki, Appl. Phys. Lett. **92**, 162504 (2008).
[53] A. Bhattacharya, S. J. May, S. G. E. te Velthuis, M. Warusawithana, X. Zhai, B. Jiang, J.-M. Zuo, M. R. Fitzsimmons, S. D. Bader, and J. N. Eckstein, Phys. Rev. Lett. **100**, 257203 (2008).
[54] C. Adamo, X. Ke, P. Schiffer, A. Soukiassian, M. Warusawithana, L. Maritato, and D. G. Schlom, Appl. Phys. Lett. **92**, 112508 (2008).
[55] H. Boschker, M. Huijben, A. Vailionis, J. Verbeeck, S. van Aert, M. Luysberg, S. Bals, G. van Tendeloo, E. P. Houwman, G. Koster, D. H. A. Blank, and G. Rijnders, J. Phys. D: Appl. Phys. **44**, 205001 (2011).
[56] A. Urushibara, Y. Moritomo, T. Arima, A. Asamitsu, G. Kido, and Y. Tokura, Phys. Rev. B **51**, 14103 (1995).
[57] J.-B. Yau, X. Hong, A. Posadas, C. H. Ahn, W. Gao, E. Altman, Y. Bason, L. Klein, M. Sidorov, and Z. Krivokapic, J. Appl. Phys. **102**, 103901 (2007).
[58] See Supplemental Material at http://link.aps.org/supplemental/10.1103/PhysRevB.95.155135 for comparison of two- and four-point probe resistance measurements of LSMO/STO.
[59] M. F. Hundley, M. Hawley, R. H. Heffner, Q. X. Jia, J. J. Neumeier, J. Tesmer, J. D. Thompson, and X. D. Wu, Appl. Phys. Lett. **67**, 860 (1995).
[60] Y. Tokura and Y. Tomioka, J. Magn. Magn. Mater. **200**, 1 (1999).
[61] M. Ge, T. F. Qi, O. B. Korneta, D. E. De Long, P. Schlottmann, W. P. Crummett, and G. Cao, Phys. Rev. B **84**, 100402(R) (2011).
[62] J.-H. Park, E. Vescovo, H.-J. Kim, C. Kwon, R. Ramesh, and T. Venkatesan, Phys. Rev. Lett. **81**, 1953 (1998).
[63] J. J. Kavich, M. P. Warusawithana, J. W. Freeland, P. Ryan, X. Zhai, R. H. Kodama, and J. N. Eckstein, Phys. Rev. B **76**, 014410 (2007).
[64] F. Yang, N. Kemik, M. D. Biegalski, H. M. Christen, E. Arenholz, and Y. Takamura, Appl. Phys. Lett. **97**, 092503 (2010).
[65] F. Hellman, A. Hoffmann, Y. Tserkovnyak, G. S. D. Beach, E. E. Fullerton, C. Leighton, A. H. MacDonald, D. C. Ralph, D. A. Arena, H. A. Dürr, P. Fischer, J. Grollier, J. P. Heremans, T. Jungwirth, A. V. Kimel, B. Koopmans, I. N. Krivorotov, S. J. May, A. K. Petford-Long, J. M. Rondinelli, N. Samarth, I. K. Schuller, A. N. Slavin, M. D. Stiles, O. Tchernyshyov, A. Thiaville, and B. L. Zink, arXiv:1607.00439 [Rev. Mod. Phys. (to be published)].